Caging and fluid deformations in dense bidisperse suspensions

Virgile Thiévenaz and Nathan Vani

PMMH, CNRS, ESPCI Paris, Université PSL, Sorbonne Université, Université Paris Cité, F-75005, Paris, France

Alban Sauret

Department of Mechanical Engineering, University of California, Santa Barbara, California 93106, USA

(Dated: November 14, 2023)

We investigate the link between the geometric environment of particles, the local deformations of the solvent, and the bulk effective viscosity in non-Brownian suspensions. First, we discuss the caging of particles by their neighbors, and especially the caging of small particles by large ones in bidisperse suspensions. We develop a model that attributes an effective volume to particles depending on their environment, and yields the local deformations and effective viscosity. We compare this model to data from the literature, as well as to our own experiments with suspensions of non-Brownian polystyrene beads. Using dissolved polymers and their coil-stretch transition as strain probes, we measure the local deformation of the liquid and the effect of caging thereon. We obtain a linear relationship between the amplified local strain rate and the particle volume fraction, in which the critical volume fraction ϕ_c appears as an effective volume of the particles; this relationship is found valid up into the dense regime.

Many fluids in nature and industry are suspensions of solid particles in a liquid [1], and as such are a challenge to describe in terms of continuous media [2]. Rigid particles deform the flow and increase the stress applied on the liquid [3]. As a result, the suspension exhibits an effective viscosity η_s which may be orders of magnitude higher than that of the liquid η_0 [4]. Many semi-empirical laws describe how the relative viscosity $\eta_r = \eta_s/\eta_0$ increases with the volume fraction of solid ϕ [5–7]; for example that of Maron and Pierce [8]: $\eta_r = (1 - \phi/\phi_c)^{-2}$. All introduce an empirical parameter ϕ_c, described as the critical volume fraction at which the viscosity diverges. It is remarkable that these laws describe well many different suspensions – particles of different sizes and materials [4], of different shapes [9], in different solvents [10] – all the differences being contained in this parameter ϕ_c.

Polydispersity plays a crucial role, and most common suspensions are polydisperse, meaning their grains have a range of size. Such suspensions are less viscous than ideal monodisperse suspensions of equal volume fraction [11, 12]. Recent studies on the flow of bidisperse suspensions (containing particles of two different sizes) have shown that a minute amount of particles of a second size can change the dynamics significantly [13–15], by modifying the scale of collective motion [16]. Shear-induced migration [17] causes segregation when a bidisperse suspension flows confined in a channel [18, 19]. The Wyart-Cates model [20], which explains shear-thickening as a transition from frictionless to frictional contacts, is successful at describing monodisperse suspensions but fails with bidisperse suspensions [21]. Even bidisperse active matter shows peculiar behavior because of differentiated interactions between small and large particles [22]. Despite this apparent complexity, the same empirical laws match the viscosity of bidisperse suspensions and simply yield other values of ϕ_c [23]. How to estimate ϕ_c, and how it relates to the jamming transition, remain open questions.

In this Letter, we investigate the local environment of particles in bidisperse non-Brownian suspensions, especially the caging of small particles by large ones. We infer a model for the local strain rate. Then, using the coil-stretch transition of dissolved polymers as a strain probe [24, 25], we measure the local strain rate in the liquid phase. Finally, we discuss the effect of caging on the macroscopic viscosity. For the sake of clarity, we begin by describing the model before our experiments and their discussion.

The model consists in attributing an effective volume to each particle, so that the suspension can be seen as an effective packing of spherical cells. Each cell contains a particle and some surrounding fluid; the solid volume fraction is ϕ, the fraction of effective volume is $\phi^\star$. Particles are rigid, only the liquid may deform. Therefore, when the suspension deforms at a macroscopic strain rate $\dot{\varepsilon}$, the liquid deforms at an increased local strain rate $\dot{\varepsilon}_{\mathrm{loc}}$ (Fig. 1a). We consider that the strain rate can be averaged over the effective volume, so the total deformation is $\dot{\varepsilon}\phi^\star = \dot{\varepsilon}_{\mathrm{loc}}(\phi^\star - \phi)$, hence

$$\dot{\varepsilon}_{\mathrm{loc}}(\phi)/\dot{\varepsilon} = (1 - \phi/\phi^\star)^{-1}. \qquad (1)$$

Eq. (1) was obtained by Mills and Snabre following similar arguments [26, 27] and served as an hypothesis to build more complex rheological models. We shall demonstrate that this equation is directly validated by experiments by measuring both $\dot{\varepsilon}$ and $\dot{\varepsilon}_{\mathrm{loc}}$. But first, we discuss how the effective volume vary in bidisperse suspensions.

A bidisperse suspension contains particles of two different sizes; large ones of diameter d_{L} and volume fraction ϕ_{L}, and small ones of diameter d_{S} and volume fraction ϕ_{S}; $\phi = \phi_{\mathrm{S}} + \phi_{\mathrm{L}}$. We introduce the size ratio of the particles $\delta = d_{\mathrm{L}}/d_{\mathrm{S}}$, the size ratio of the cells $\hat{\delta} = \hat{d_{\mathrm{L}}}/\hat{d_{\mathrm{S}}}$,
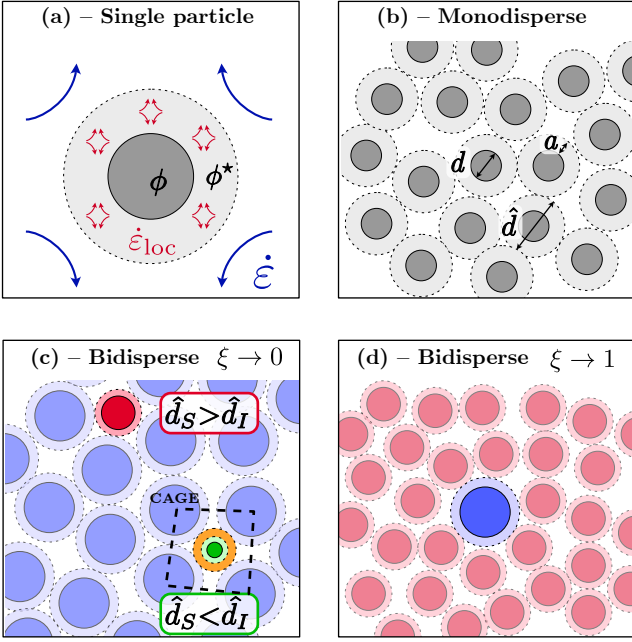
FIG. 1. (a) Amplification of the macroscopic strain rate $\dot{\varepsilon}$ near the particle; within the effective volume $\phi^{\star}$, the strain rate in increased up to $\dot{\varepsilon}_{\mathrm{loc}}$. (b) Monodisperse suspension of spheres (dark gray) and their effective volume (light gray). (c) Bidisperse suspension with many large particles and few small ones ($\xi \to 0$). Depending on the relative size of the small particles d_{S} and of the interstices between the large particles d_{I}, the small particles may (in green) or may not (in red) be caged by the large ones. In the former case, the small particles have an effective volume equal to that of the interstice (in orange). (d) Bidisperse suspension with few large particles and many small ones ($\xi \to 1$).

and the share of small particles $\xi = \phi_{\mathrm{S}}/\phi$. In a monodisperse suspension, all cells have on average the same size (Fig. 1b); each cell contains one particle of diameter d and the layer of liquid of thickness a, so the cell diameter is simply $\hat{d} = d + 2a$. In a bidisperse suspension, a may depend on the size and local environment of the particle considered, so $\hat{d}_i = d_i + 2a_i$ where i refers to a given particle. The average effective volume of the bidisperse suspension is then the compacity of the packing of the bidisperse cells $\phi_2^{\star}$. We compute it using the model of Ouchiyama and Tanaka [28, 29], which consists in evaluating the local compacity around a given sphere surrounded with spheres of the average size, and then taking the average over the size distribution. This model has been adapted to bidisperse packings [13, 23], and agrees well with measurements for dry grains [30]. Thanks to it, $\phi_2^{\star}$ can be related to the compacity of a monodisperse packing $\phi_1^{\star}$:

$$\phi_2^{\star} = f(\phi_1^{\star}, \hat{\delta}, \xi). \tag{2}$$

Since the full expression of $\phi_2^{\star}$ is quite long and not necessary for the discussion, we leave it to the supplementary

material [31].

Eq. (2) requires that we know $\hat{\delta}$. There are two different cases, depending on whether the small particles are large enough to disturb the packing of large cells, or are small enough to sit in the interstices between the large cells. For particles of similar size ($\delta \simeq 1$), we assume that a_i is simply proportional to d_i; $a_{\mathrm{L}}/d_{\mathrm{L}} = a_{\mathrm{S}}/d_{\mathrm{S}}$. The size ratio of cells is then equal to the size ratio of particles: $\hat{\delta} = \delta$. Physically, this means that the small particles experience the same environment as the large ones.

If the small particles are small enough, their cells may sit in the interstices between large cells. Such interstices should be surrounded by six large cells on average, two per dimension of space. Assuming the interstice has no privileged direction, it should be an octaedric site, of diameter $\hat{d}_{\mathrm{I}} = \left(\sqrt{2} - 1\right)\hat{d}_{\mathrm{L}}$. The size ratio of the large cell to the interstitial cell is then :

$$\hat{\delta}_{\mathrm{I}} = \hat{d}_{\mathrm{L}}/\hat{d}_{\mathrm{I}} = \left(\sqrt{2} - 1\right)^{-1} \simeq 2.41. \tag{3}$$

We model the interstices as follows. There are two possible environments for a small particle: *free* among its neighbors, or *caged* by them (Fig. 1(c), respectively in red and green). We assume that if a small particle is caged in an interstice then its effective volume is the whole interstice (Fig. 1(c), green particle in orange interstice). Therefore, its effective diameter is $\hat{d}_{\mathrm{S}}$ if it is free and $\hat{d}_{\mathrm{I}}$ if it is caged. Only small particles can be caged, but if there are more small particles than cages, then some small particles will be free. Assuming there are as many interstices as large cells, the average effective diameter of the small particles is:

$$\hat{d}_{\mathrm{S}}(\xi) = \xi(\hat{d}_{\mathrm{L}}/\delta) + (1 - \xi)\hat{d}_{\mathrm{I}}. \tag{4}$$

Therefore, the general expression of the size ratio of cells is:

$$\hat{\delta} = \delta \quad \text{for} \quad \delta \leq \hat{\delta}_{\mathrm{I}}; \tag{5}$$

$$\hat{\delta} = \frac{\delta\hat{\delta}_{\mathrm{I}}}{\xi\hat{\delta}_{\mathrm{I}} + (1 - \xi)\delta} \quad \text{for} \quad \delta > \hat{\delta}_{\mathrm{I}}. \tag{6}$$

In the limit $\xi \to 1$, both equations are equivalent; it means that if there are few large particles, caging the small ones is impossible (Fig. 1d). Eqs. (5-6) together with Eq. (2) enable to compute the effect of caging on the effective volume in bidisperse suspensions. The local strain rate and the bulk viscosity can thence be deduced.

Our original measure of the local strain rate $\dot{\varepsilon}_{\mathrm{loc}}$ consists in adding minute amounts of polymer dissolved in the liquid phase and then stretching the suspension. A most simple stretching experiment consists in observing the detachment of a drop (Figure 2a and b). At rest, polymer chains are coiled since this conformation maximizes their entropy; above a critical rate of strain the
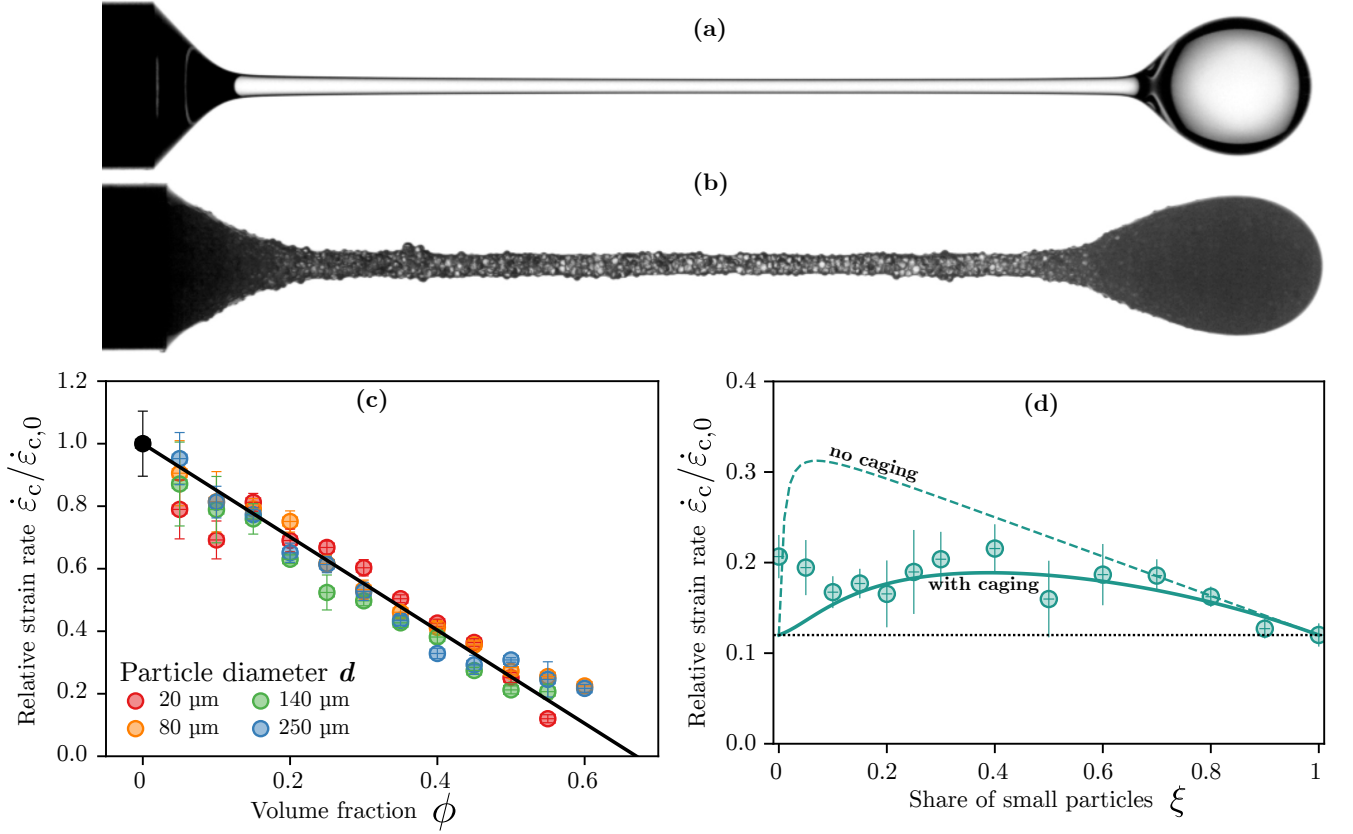
FIG. 2. (a) Stretching of a polymer solution. The nozzle is 5.5 mm-wide. (b) Same experiment with 250 μm-polystyrene particles at $\phi = 60\%$. (c) Amplification of the local rate of strain $\dot{\varepsilon}_c/\dot{\varepsilon}_{c,0}$ *vs.* volume fraction for monodisperse suspensions. (d) $\dot{\varepsilon}_c/\dot{\varepsilon}_{c,0}$ *vs.* the share of small particles ξ in bidisperse suspensions, with $d_S = 20$ μm and $d_L = 140$ μm, at constant $\phi = 55\%$. Lines represent the model including the caging effect (solid line) and excluding it (dashed line).

chains unwind and stretch; this is the coil-stretch transition [32, 33]. Macroscopically, the thinning of a polymer solution switches from a Newtonian to a viscoelastic regime [34], through a universal transition that is only controlled by the critical macroscopic strain rate $\dot{\varepsilon}_c$ [25]. With particles (large compared to the polymer chains) in the solution, the transition occurs for a lower $\dot{\varepsilon}_c$, meaning that the polymer chains undergo higher stress [24]. Therefore, by comparing the critical strain rate for the suspension $\dot{\varepsilon}_c$ and for the polymer solution without particles $\dot{\varepsilon}_{c,0}$, we can measure by how much particles amplify the local strain.

The polymer solution is polyethylene oxide (PEO, Sigma) of molar weight $4 \cdot 10^6$ mol/kg, dissolved at a weight fraction of 0.02% in a 75%-water, 25%-glycerol mixture. It is gently stirred on a roller mixer during two days to ensure uniform concentration, and then mixed with the particles. We used polystyrene beads (Dynoseeds from Microbeads) of four different diameters (20, 80, 140 and 250 μm) [31]. For the stretching experiments, the suspensions were extruded through a 5.5 mm-wide nozzle. Based on our previous work [24, 25], this system satisfies the following constraints: neutrally-

buoyant particles; sharp transition to the viscoelastic regime to maximize the precision on $\dot{\varepsilon}_c$; macroscopic transition to the viscoelastic regime at flow scales much larger than the particle size, to avoid confinement [31]. The thinning dynamics are recorded using a high-speed camera (Phantom VEO 710) and a macro lens (Nikon Micro-Nikkor AI-s 200mm f/4). The macroscopic strain rate $\dot{\varepsilon}(t)$ is computed from the thickness $h(t)$ of the liquid thread at its thinnest point; $\dot{\varepsilon}(t) = -2\,\mathrm{d}(\log h)/\mathrm{d}t$ [31]; The critical strain rate $\dot{\varepsilon}_c$ is the maximum value of $\dot{\varepsilon}$. Each experiment was repeated ten times to reduce uncertainty.

Using this protocol, we measured $\dot{\varepsilon}_c$ for monodisperse suspensions with volume fraction ϕ ranging from 5% to 60%, and for the solution without particles: $\dot{\varepsilon}_{c,0} = \dot{\varepsilon}_c(\phi = 0)$. Since the coil-stretch transition is caused by the flow at the scale of the polymer chains, which is much smaller than the particles, the local strain rate $\dot{\varepsilon}_{loc}$ should have the same value in all experiments; therefore $\dot{\varepsilon}_{loc} = \dot{\varepsilon}_{c,0}$. Figure 2(c) shows that the ratio $\dot{\varepsilon}_c/\dot{\varepsilon}_{c,0}$ follows a linear decrease: $\dot{\varepsilon}_c/\dot{\varepsilon}_{c,0} = 1 - \phi/\phi^\star$; the best fit gives $\phi^\star = 67\%$. We observe no effect of the particle size. Since $\dot{\varepsilon}_c/\dot{\varepsilon}_{c,0}$ is the ratio of macroscopic to local strain rate, this is a
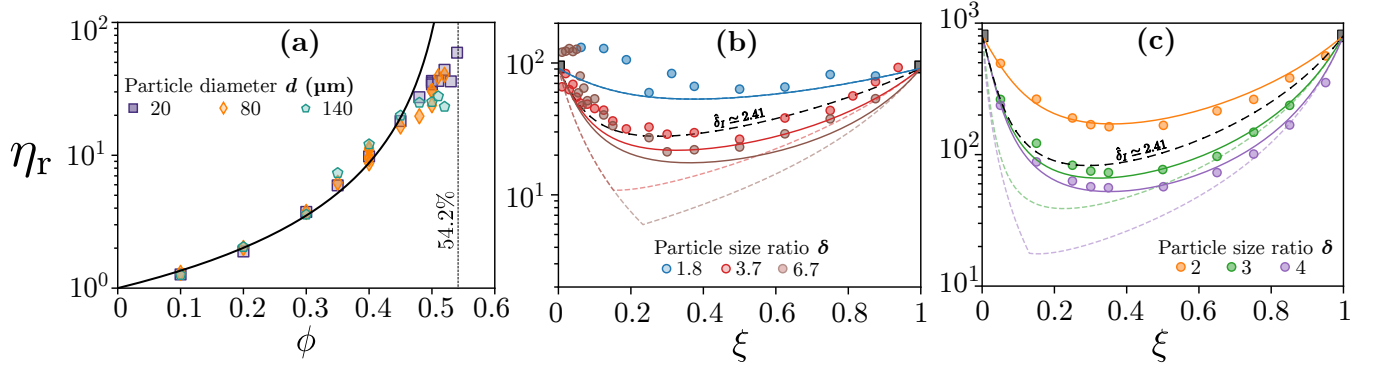
FIG. 3. (a) Relative viscosity η_r of monodisperse suspensions *vs.* volume fraction ϕ; the line indicates the best fit by Eq. (8). (b) η_r *vs.* the share of small particles ξ for bidisperse suspensions at $\phi = 50\%$. (c) Comparisons with the simulations of Pednekar *et al.* [12] for $\phi = 60\%$. For both (b) and (c), solid lines represent the predictions of the model. Colored dashed lines represent the prediction not taking caging into account. The black dashed lines represent the case $\hat{\delta} = \hat{\delta}_I$, *i.e.* the asymptotical regime $\xi \to 0$.

direct validation of Eq. (1), which is therefore no longer an hypothesis but an experimental fact. It must be emphasized that Eq. (1) is valid throughout the whole range of volume fractions, from 5% up to 60%.

This method can be extended to bidisperse suspensions by mixing beads of two sizes in the same polymer solution. We conducted many experiments with various particle size couples and different volume fractions, but because the effect of the size distribution on $\dot{\varepsilon}_c$ is weak we could only observe it in the most concentrated case ($\phi = 55\%$) with the highest size ratio ($\delta = 6.7$, see Fig. 2(d)). It should be noted that for such a high size ratio caging should be important. The full line represents the prediction of Eqs. (2-6), in very good agreement with the data. The value of $\phi_1^\star$ is taken to match the value of the point at $\xi = 1$. The dashed line represents the prediction not taking caging into account, that is taking cell sizes proportional to particle sizes; it is off by a factor 2. Caging is therefore important. The less good agreement when $\xi \to 0$ is likely due to our hypothesis that $\phi_1^\star$ is exactly the same for the different sizes; the difference is small yet not completely negligible.

Although the experimental measurement of the strain rate is quite useful, the usually measured quantity is the viscosity of the suspension η_s. It may be derived by writing that the power dissipated per unit volume of suspension equals the power dissipated per unit volume of liquid multiplied by the volume fraction of liquid:

$$\eta_s \dot{\varepsilon}^2 = (1 - \phi)\eta_0 \dot{\varepsilon}_{loc}^2, \tag{7}$$

hence the relative viscosity [26]:

$$\eta_r = \frac{\eta_s}{\eta_0} = \frac{1 - \phi}{(1 - \phi/\phi^\star)^2}. \tag{8}$$

We measured the shear viscosity of suspensions of the same polystyrene beads, dispersed in a mixture of water and polyethylene glycol (58%-42% wt.). This liquid

has the same density as the beads ($1050 \, \text{kg/m}^3$); it is Newtonian at the shear rate considered and its viscosity is $103 \, \text{mPa} \cdot \text{s}$. The rheometer (Anton Paar MCR92) is equipped with a plane-plane geometry with rough surfaces to avoid slippage; the gap between the plates is 1 mm. The viscosity is measured in the stationary regime under an imposed shear rate of $100 \, \text{s}^{-1}$. For monodisperse suspensions, Eq. (8) matches our measurements up to $\phi \simeq 48\%$; the best fit in this range yields $\phi^\star = 54.2\%$ (Fig. 3a), the same value for the three particle sizes. For bidisperse suspensions, we compare our model to viscosity measurements for $\phi = 50\%$ (Fig. 3b); we obtain a fair agreement with our experiments, taking $\phi_1^\star = 54.2\%$ as measured on monodisperse suspensions. The most remarkable result comes from the comparison with the numerical simulations of Pednekar *et al.* [12] (Fig. 3c), which describe the most concentrated case of $\phi = 60\%$. For $\delta = 2$ (orange), the agreement is perfect; it should be noted that in this case there is no caging, since $\delta < \hat{\delta}_I$. We obtain a very good agreement as well for $\delta = 3$ and 4, when there is caging. In these cases we also plot the prediction that would be made were caging neglected (colored dashed lines), which is off by an order of magnitude. The corresponding value of $\phi_1^\star$ is 0.6137. The model compares as well [31] to other data from the literature [23, 35].

Throughout the paper, we have considered the effective volume of the particles, and its average $\phi^\star$ over the size distribution. It follows from Eq. (8) that $\phi^\star$ is very similar to the ϕ_c of the viscosity laws, although its interpretation is different. $\phi^\star$ is a measure of the topology of the microstructure, and as such it depends on the flow that produces it. It is therefore not surprising to obtain different values of $\phi^\star$ between pinch-off and rheometer experiments; what matters is the variation of $\phi^\star$ within a given experiment. Although jamming would of course affect its value, it has a physical meaning far from the jamming transition (our experiments include the dilute

range $\phi \leq 10\%$): the effective volume in which particles amplify the fluid deformations.

The caging of small particles by large ones has an important effect on the local strain rate and on the bulk viscosity, especially when there are few small particles. Caging occurs when small particles can be trapped in the interstices between the large ones, that is when the size ratio is greater than $\hat{d}_{\mathrm{I}} \simeq 2.41$. Because of its basic hypotheses, our model is only valid at low shear rates. In the general case, one should take into account the more complex shape of the interstices, due to shear breaking symmetry, as well as the kinetics of caging and freeing.

The good agreement between our model – that does not consider any kind of deformation nor dissipation due to solid friction between particles – and the various rheological data presented here suggests that the work of friction forces is negligible in our system, in agreement with contact force measurements [10]. However, this does not mean that friction is negligible, or that there are no contacts, but only that these act principally by reducing particle mobility, hence hindering the flow and increasing viscous dissipation [36, 37]. The question remains open for high shear rates, typically in the case of shear-thickening. One would need to experimentally measure the fluid deformation in a suspension undergoing shear-thickening, maybe using dissolved polymers.

———————

[1] R. Kostynick, H. Matinpour, S. Pradeep, S. Haber, A. Sauret, E. Meiburg, T. Dunne, P. Arratia, and D. Jerolmack, Rheology of debris flow materials is controlled by the distance from jamming, Proceedings of the National Academy of Sciences **119**, e2209109119 (2022).

[2] C. Ness, R. Seto, and R. Mari, The physics of dense suspensions, Annual Review of Condensed Matter Physics **13**, 97 (2022).

[3] A. Einstein, *Eine neue bestimmung der moleküldimensionen*, Ph.D. thesis, ETH Zurich (1905).

[4] É. Guazzelli and O. Pouliquen, Rheology of dense granular suspensions, Journal of Fluid Mechanics **852** (2018).

[5] v. H. Eilers, Die viskosität von emulsionen hochviskoser stoffe als funktion der konzentration, Kolloid-Zeitschrift **97**, 313 (1941).

[6] I. M. Krieger and T. J. Dougherty, A mechanism for non-newtonian flow in suspensions of rigid spheres, Transactions of the Society of Rheology **3**, 137 (1959).

[7] N. Frankel and A. Acrivos, On the viscosity of a concentrated suspension of solid spheres, Chemical Engineering Science **22**, 847 (1967).

[8] S. H. Maron and P. E. Pierce, Application of ree-eyring generalized flow theory to suspensions of spherical particles, Journal of Colloid Science **11**, 80 (1956).

[9] S. N. Bounoua, P. Kuzhir, and E. Lemaire, Shear reversal experiments on concentrated rigid fiber suspensions, Journal of Rheology **63**, 785 (2019).

[10] A. V. Nguyen Le, A. Izzet, G. Ovarlez, and A. Colin, Solvents govern rheology and jamming of polymeric bead suspensions, Journal of Colloid and Interface Science **629**, 438 (2023).

[11] A. P. Shapiro and R. F. Probstein, Random packings of spheres and fluidity limits of monodisperse and bidisperse suspensions, Physical Review Letters **68**, 1422 (1992).

[12] S. Pednekar, J. Chun, and J. F. Morris, Bidisperse and polydisperse suspension rheology at large solid fraction, Journal of Rheology **62**, 513 (2018).

[13] V. Thiévenaz, S. Rajesh, and A. Sauret, Droplet detachment and pinch-off of bidisperse particulate suspensions, Soft Matter **17**, 6202 (2021).

[14] D.-H. Jeong, M. K. H. Lee, V. Thiévenaz, M. Z. Bazant, and A. Sauret, Dip coating of bidisperse particulate suspensions, Journal of Fluid Mechanics **936** (2022).

[15] A. Pelosse, É. Guazzelli, and M. Roché, Probing dissipation in spreading drops with granular suspensions, Journal of Fluid Mechanics **955**, A7 (2023).

[16] V. Thiévenaz and A. Sauret, The onset of heterogeneity in the pinch-off of suspension drops, Proceedings of the National Academy of Sciences **119**, e2120893119 (2022).

[17] M. Lyon and L. Leal, An experimental study of the motion of concentrated suspensions in two-dimensional channel flow. part 1. monodisperse systems, Journal of Fluid Mechanics **363**, 25 (1998).

[18] M. Lyon and L. Leal, An experimental study of the motion of concentrated suspensions in two-dimensional channel flow. part 2. bidisperse systems, Journal of Fluid Mechanics **363**, 57 (1998).

[19] A. Nath and A. Sen, Flow of bidisperse suspensions under the effect of standing bulk acoustic waves, Physical Review Fluids **7**, 104201 (2022).

[20] M. Wyart and M. Cates, Discontinuous shear thickening without inertia in dense non-brownian suspensions, Physical Review Letters **112**, 098302 (2014).

[21] B. M. Guy, C. Ness, M. Hermes, L. J. Sawiak, J. Sun, and W. C. Poon, Testing the wyart–cates model for non-brownian shear thickening using bidisperse suspensions, Soft Matter **16**, 229 (2020).

[22] S. Maity and A. Morin, Spontaneous demixing of binary colloidal flocks, Physical Review Letters **131**, 178304 (2023).

[23] P. Gondret and L. Petit, Dynamic viscosity of macroscopic suspensions of bimodal sized solid spheres, Journal of Rheology **41**, 1261 (1997).

[24] V. Thiévenaz and A. Sauret, Pinch-off of viscoelastic particulate suspensions, Physical Review Fluids **6**, L062301 (2021).

[25] S. Rajesh, V. Thiévenaz, and A. Sauret, Transition to the viscoelastic regime in the thinning of polymer solutions, Soft Matter **18**, 3147 (2022).

[26] P. Mills, Non-newtonian behaviour of flocculated suspensions, Journal de Physique Lettres **46**, 301 (1985).

[27] P. Mills and P. Snabre, The fractal concept in the rheol-

ogy of concentrated suspensions, in *Progress and Trends in Rheology II*, 26 (Rheologica Acta, 1988) pp. 105–108.

[28] N. Ouchiyama and T. Tanaka, Porosity of a mass of solid particles having a range of sizes, Industrial & Engineering Chemistry Fundamentals **20**, 66 (1981).

[29] N. Ouchiyama and T. Tanaka, Porosity estimation for random packings of spherical particles, Industrial & Engineering Chemistry Fundamentals **23**, 490 (1984).

[30] D. M. Kalyon and S. Aktaş, Factors affecting the rheology and processability of highly filled suspensions, Annual Review of Chemical and Biochemical Engineering **5**, 229 (2014).

[31] see supplementary material.

[32] P. De Gennes, Coil-stretch transition of dilute flexible polymers under ultrahigh velocity gradients, The Journal of Chemical Physics **60**, 5030 (1974).

[33] D. E. Smith, H. P. Babcock, and S. Chu, Single-polymer dynamics in steady shear flow, Science **283**, 1724 (1999).

[34] Y. Amarouchene, D. Bonn, J. Meunier, and H. Kellay, Inhibition of the finite-time singularity during droplet fission of a polymeric fluid, Physical Review Letters **86**, 3558 (2001).

[35] C. Chang and R. L. Powell, Effect of particle size distributions on the rheology of concentrated bimodal suspensions, Journal of Rheology **38**, 85 (1994).

[36] S. Jamali and J. F. Brady, Alternative frictional model for discontinuous shear thickening of dense suspensions: Hydrodynamics, Physical Review Letters **123**, 138002 (2019).

[37] M. Wang, S. Jamali, and J. F. Brady, A hydrodynamic model for discontinuous shear-thickening in dense suspensions, Journal of Rheology **64**, 379 (2020).

Caging and fluid deformations in dense bidisperse suspensions
Supplementary Material

Virgile Thiévenaz and Nathan Vani

PMMH, CNRS, ESPCI Paris, Université PSL, Sorbonne Université, Université Paris Cité, F-75005, Paris, France

Alban Sauret

Department of Mechanical Engineering, University of California, Santa Barbara, California 93106, USA
(Dated: November 14, 2023)

MOVIES

Movie 1 and Movie 2 respectively correspond to the experiments shown on Figure (2a) and Figure (2b) of the main text. Movie 3 corresponds to Figure (1) of the supplementary material.

I. PINCH-OFF OF DROP OF SUSPENSIONS CONTAINING DISSOLVED POLYMERS

In this section, we recall the principles of the pinch-off experiments that enable us to measure the local strain rate. For further details, we refer the reader to references [1, 2]. Figure 1 describes a typical experiment with 140 μm-particles, at volume fraction 40%. For each droplet detachment experiment, we measure the thickness at the thinnest point of the neck $h(t)$ on the video. During the detachment, h goes through two distinct regimes. The first one is Newtonian, and corresponds to the balance of surface tension and inertia; dimensional analysis leads to the scaling law $h(t) \propto (t - t_c)^{2/3}$, with t_c the time when pinch-off should occur were there no polymer (orange line in Fig. 1). Viscosity may play a minor role acting on the prefactor of the scaling law [1]. Because the dissolved polymer chains
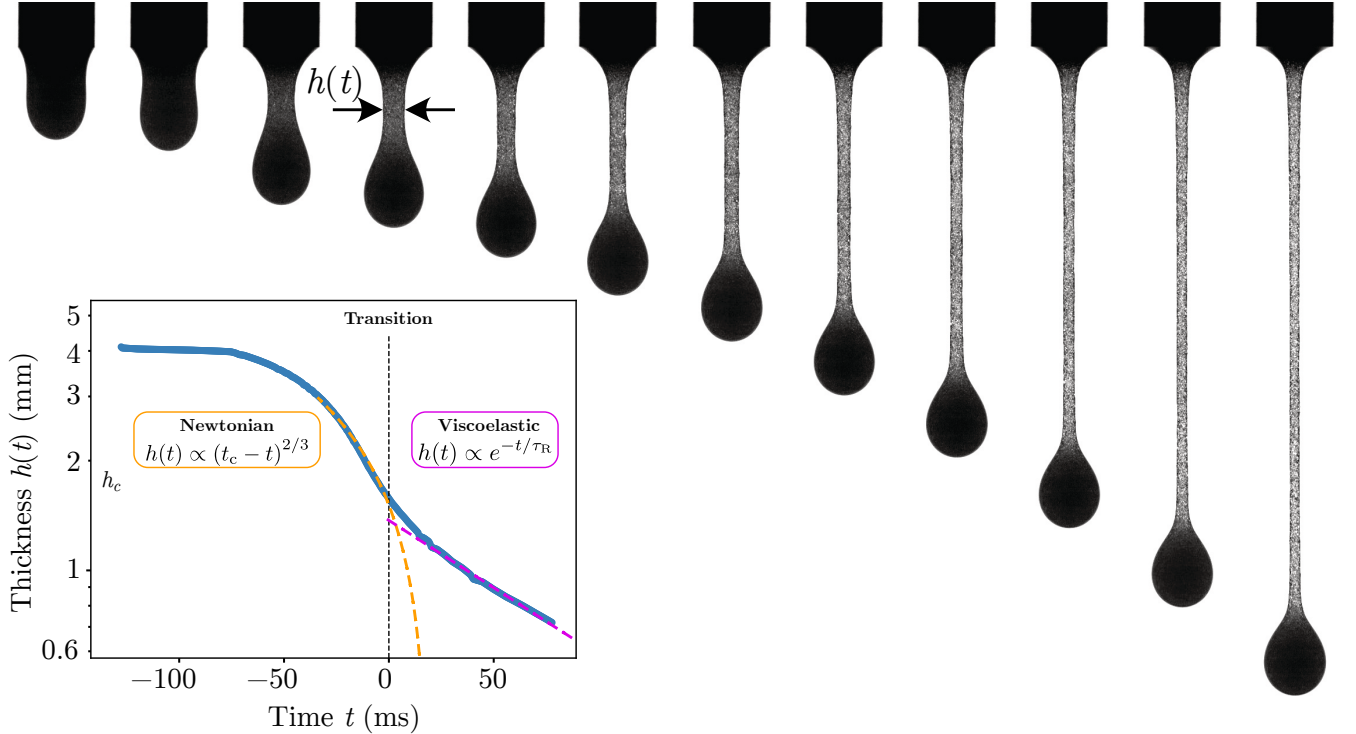

FIG. 1. Time lapse of the detachment of a suspension of polystyrene beads in a solution. The whole process takes 220 ms; starting from the third one on, pictures are equally spaced by 10 ms. Inset: thickness at the thinnest point h *vs.* time. The colored dashed lines represent the two classical regimes: Newtonian (in orange), and viscoelastic (in purple). The y-axis has a logarithmic scale so the latter regime appears as a straight line.
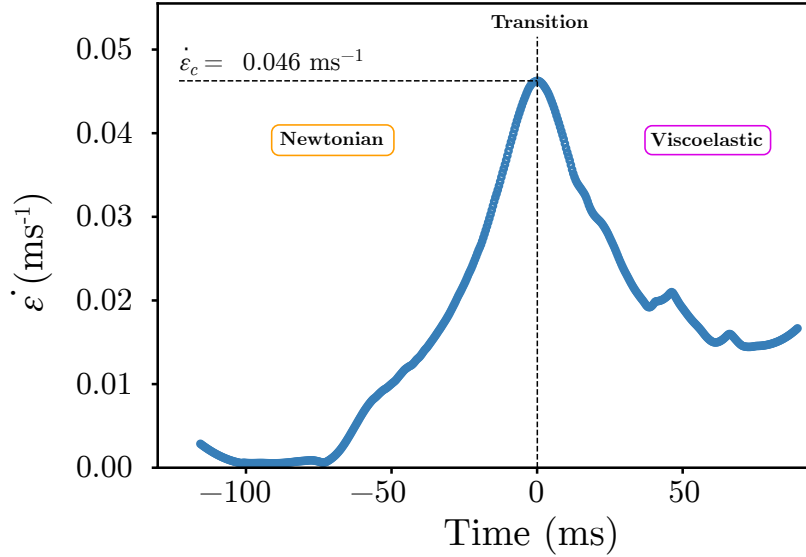
FIG. 2. Macroscopic rate of strain, measured at the thinnest point, *vs.* time.

react to high stress by stretching, the Newtonian regime gives way to the viscoelastic regime, where the dynamics follows $h(t) \propto e^{-t/\tau_\mathrm{R}}$ (purple line in Fig. 1). The relaxation time τ_R equals 117 ms for the given experiment.

From the measurements of $h(t)$, we compute the macroscopic rate of strain at the thinnest point, where the strain rate is maximum:

$$\dot{\varepsilon}(t) = -2\frac{\mathrm{d}}{\mathrm{d}t}(\log h) \tag{1}$$

Around the transition to the viscoelastic regime, the curve $\dot{\varepsilon} = f(t)$ has a similar form in all experiments, with a maximum $\dot{\varepsilon}_\mathrm{c}$ at the transition (Fig. 2). We measure $\dot{\varepsilon}_\mathrm{c}$ for each experiment. The transition is more or less sharp depending on the parameters, but all experiments can be rescaled onto a single master curve by taking $\dot{\varepsilon}_\mathrm{c}$ as scale for the rate of strain and $\dot{\varepsilon}_\mathrm{c}^{-1}$ as the time scale [2].

This experiment was developed after our previous work on the pinch-off of suspension drops with a polymer solution as solvent [1]. In the latter, we encountered problems using the larger particles (140 and 250 µm), which we attribute to confinement effects. The thickness of the neck at the transition h_c was, in these experiments, on average equal to 210 µm, much too close to the particle diameter. After our dedicated study on the transition to viscoelasticity [2], we have been able to choose the polymer, the solvent and the nozzle size so as to obtain a larger thickness at the transition; in the current experiments h_c varies between 1 and 2 mm. As a result, and as is shown in Figure (2) of the main text, $\dot{\varepsilon}_\mathrm{c}/\dot{\varepsilon}_\mathrm{c,0}$ does not depend on the particle diameter as it did in our previous study. Particle diameter is irrelevant because confinement is negligible.

II. THE OUCHIYAMA-TANAKA MODEL FOR BIDISPERSE SPHERE PACKINGS

The Ouchiyama-Tanaka model [3, 4] considers a packing of spheres having a range of sizes. Around a given sphere of a given size, one assumes that the local compacity can be approximated by considering that the neighbors of this spheres are of the average size of the distribution. The compacity of the packing ϕ_c is obtained by averaging the local compacity over the size distribution. Ouchiyama and Tanaka derived the expression of ϕ_c for an arbitraty continuous size distribution [3] and for a discrete size distribution [4]. The latter was adapted to a bidisperse distribution by Gondret and Petit [5]. The expression used here is given by Thiévenaz and Sauret [6]. Using the present notations, the compacity of a bidisperse sphere packing $\phi_2^\star$ is expressed as a function of the compacity of a monodisperse sphere packing $\phi_1^\star$, the size ratio of the spheres $\hat{\delta}$ and the share of the small particles in the solid phase ξ:

$$\phi_2^\star(\phi_1^\star, \hat{\delta}, \xi) = \frac{N_\mathrm{S} D_\mathrm{S}^3 + N_\mathrm{L} D_\mathrm{L}^3}{N_\mathrm{S} \frac{(D_\mathrm{S}+1)^3}{\Gamma} + N_\mathrm{L}\left((D_\mathrm{L}-1)^3 + \frac{[(D_\mathrm{L}+1)^3-(D_\mathrm{L}-1)^3]}{\Gamma}\right)}, \tag{2}$$
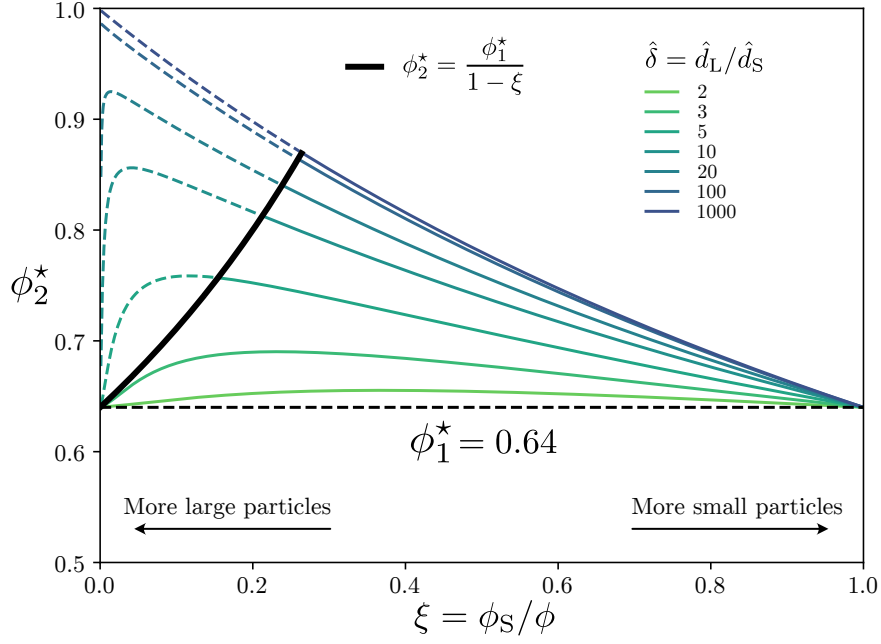
FIG. 3. Compacity of a random close packing of bidisperse spheres $\phi_2^\star$ *vs.* the share of small particles in the volume fraction ξ. Each colored curve represent the prediction of Eq. (2) for a given value of the size ratio $\hat{\delta}$, with the physical part as a solid line and the non-physical part as a dashed line. The separtion between the two parts, given by Eq. (6), is represented by the thick black solid line.

where N_S and N_L are the number fractions of small and large cells, respectively, given by:

$$N_S = \frac{\xi\hat{\delta}^3}{\xi\hat{\delta}^3 + (1-\xi)} \quad \text{and} \quad N_L = \frac{1-\xi}{\xi\hat{\delta}^3}N_S; \tag{3}$$

D_S and D_L are the reduced sizes given by:

$$D_S = \frac{\xi\hat{\delta}^3 + (1-\xi)}{\xi\hat{\delta}^3 + (1-\xi)\hat{\delta}} \quad \text{and} \quad D_L = \hat{\delta}D_S; \tag{4}$$

and parameter Γ is:

$$\Gamma = 1 + \frac{4}{13}\left(8\phi_1^\star - 1\right)\left(\frac{N_S(D_S+1)^2\left(1 - \frac{3}{8}\frac{1}{D_S+1}\right) + N_L(D_L+1)^2\left(1 - \frac{3}{8}\frac{1}{D_L+1}\right)}{N_S\,D_S^3 + N_L\left(D_L^3 - (D_L-1)^3\right)}\right) \tag{5}$$

For small ξ the prediction of Eq. (2) must be bounded [4] by

$$\phi_2^\star(\hat{\delta}, \xi) \leq \frac{\phi_1^\star}{1-\xi}. \tag{6}$$

Indeed a packing of bidisperse spheres cannot be more compact than $\phi_1^\star/(1-\xi)$, which represents the limit case in which the small spheres are small and few enough to form a independent packing of compacity $\phi_1^\star$ within the interstices of the packing of large spheres whose compacity is also $\phi_1^\star$. Figure 3 represents the compacity of the bidisperse sphere packing predicted by Eq. (2) for different values of the size ratio $\hat{\delta}$ (colors). The value taken for $\phi_1^\star$ is 64%, near the random close packing fraction. The black line represents the maximal compacity (Eq. 6). The predictions are split between the physical part $\phi_2^\star \leq \frac{\phi_1^\star}{1-\xi}$ (solid line) and the non-physical part $\phi_2^\star > \frac{\phi_1^\star}{1-\xi}$ (dashed line).

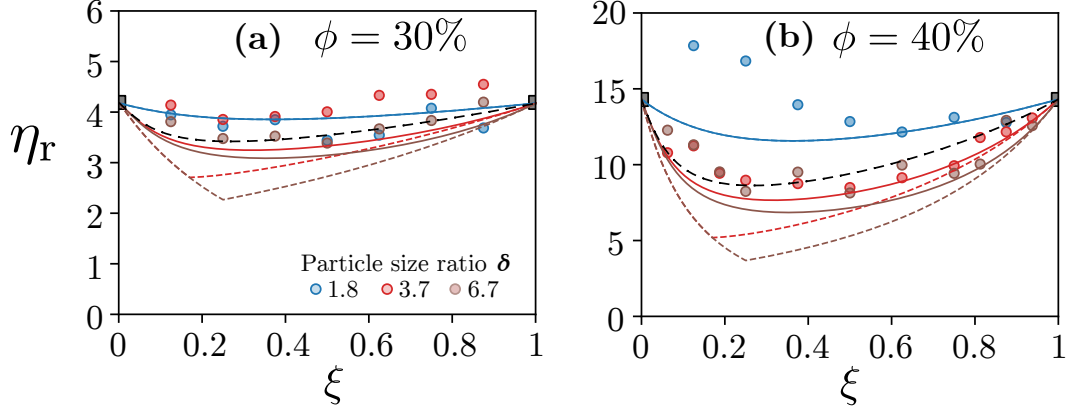## III.   FURTHER MEASUREMENTS FOR BIDISPERSE SUSPENSIONS

FIG. 4. Additional viscosity measurements at (a) $\phi = 30\%$ and (b) $\phi = 40\%$. Legend is the same as in Figure (3c) in the main text.

In addition to the viscosity measurements presented in Figure (3c) of the main text, in which the total volume fraction is constant at 50%, we also measured the viscosity of bidisperse suspensions with total volume fractions of 30% and 40% (Fig. 4). However, since the effect of polydispersity is quite weak at these volume fractions, it is not possible to confirm nor infirm the model using these data.

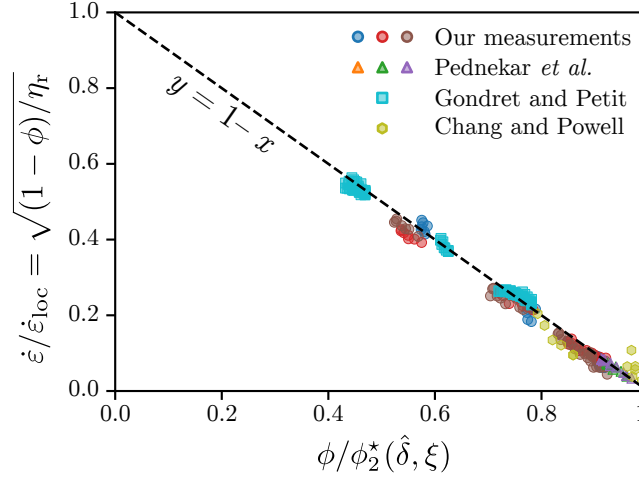## IV.   RESCALING OF THE VISCOSITY DATA

FIG. 5. Collapse of different viscosity measurements and simulations of bidisperse suspension on the same master curve. Data from Pednekar *et al.* [7], Gondret and Petit [5], and Chang and Powell [8].

Figure 5 shows the comparison between and our model data available in the literature. In addition to our measurements and the simulations of Pednekar *et al.*, we use the data of Chang & Powell [8] and of Gondret & Petit [5]. For each data set, we compute $\phi_1^\star$ by inverting the Mills-Snabre equation using the relative viscosity of the monodisperse suspension at a given volume fraction ϕ, and then compute $\phi_2^\star$ using the Ouchiyama-Tanaka model for all bidisperse suspension with the same volume fraction.

In the main text (Fig. 3c), we plot the evolution of the relative viscosity η_r with the share of small particle ξ at constant total volume fraction. Here, we provide an alternative representation of this result. The point of this Letter is to show that the local amplification of strain is the main cause of the relative viscosity increase; we may infer this amplification from the relative viscosity measurements by solving the Mills-Snabre equation for $\dot{\varepsilon}/\dot{\varepsilon}_\mathrm{loc}$. Plotting $\dot{\varepsilon}/\dot{\varepsilon}_\mathrm{loc}$

vs. the rescaled volume fraction $\phi/\phi_2^\star$ enables the collapse of all data on a most simple line of equation $y = 1 - x$. Our model thus gives an excellent agreement with the data. It should be noted that although Chang & Powell used polystyrene beads, as we do, Gondret & Petit used glass spheres whose surface physico-chemistry is *a priori* quite different; yet, this does not seems to affect the agreement with the model.

V. THE CHOICE OF THE VISCOSITY EQUATION

One could argue that the viscosity of the bidisperse suspension could be inferred from $\phi_2^\star$ using any empirical law for the viscosity; however, this is not the case. Figure 6 compares the viscosity prediction using the Mills-Snabre equation: $\eta_\mathrm{r} = (1 - \phi)/(1 - \phi/\phi^\star)^2$ (Eq. 8 in main text, Fig. 6a) the Maron-Pierce law $\eta_\mathrm{r} = (1 - \phi/\phi^\star)^{-2}$ (Fig. 6b), the Krieger-Dougherty law $\eta_\mathrm{r} = (1 - \phi/\phi^\star)^{-\frac{5}{2}\phi^\star}$ (Fig. 6c) and the Eilers law $\eta_\mathrm{r} = \left(1 + \frac{5}{4}\phi\right)/\left(1 - \phi/\phi^\star\right)^2$ (Fig. 6d), to the simulations of Pednekar *et al.* [7]. In each case, we obtain $\phi_1^\star$ by inverting the given viscosity equation using the value of the viscosity in the monodisperse case (for $\xi = 0$), then compute $\phi_2^\star(\phi_1^\star, \hat{\delta}, \xi)$ using the procedure described in the main text. The viscosity shown in Figure 6 is then computed by putting $\phi_2^\star$ in the given viscosity equation.

The Mills-Snabre equation fits best, although the more common Krieger-Dougherty equation also gives a good result; Maron-Pierce and Eilers are completely off. Therefore, the physical meaning of ϕ_c depends, unsurprisingly, on the physics that underpins the model used.
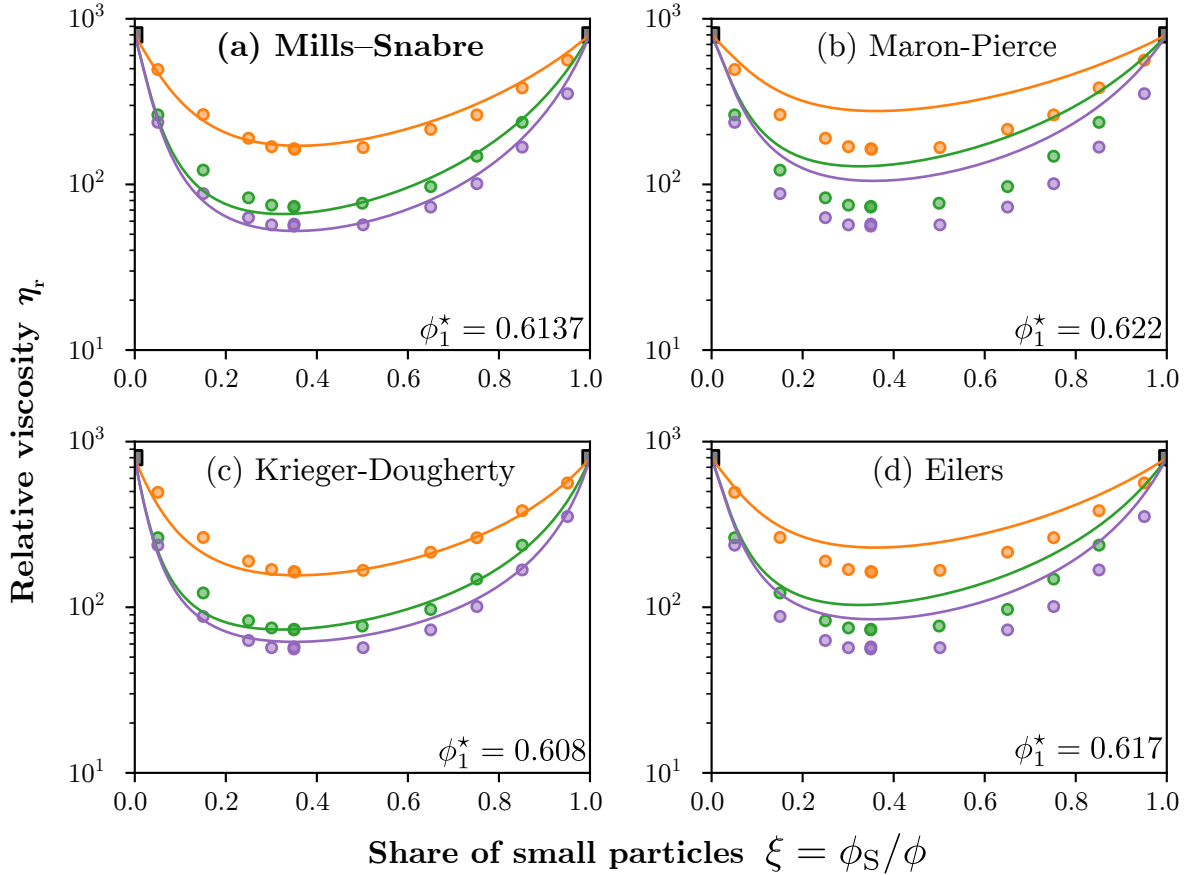

FIG. 6. Comparison of different viscosity equations to the numerical simulations of Pednekar *et al.*. The corresponding value of $\phi_1^\star$ is indicated in each sub-figure.

VI.   SIZE DISTRIBUTION OF THE POLYSTYRENE BEADS

We measured the size distribution of the polystyrene beads by taking pictures of them and measuring their individual diameters through image processing. Figure 7 shows the probability density of the diameter $f(d)$, normalized so that

$$\int_0^{+\infty} f(d)\mathrm{d}d = 1 \tag{7}$$

The distribution is well described by a gaussian distribution (dotted line) for the 20, 140 and 250-μm particles; the 80-μm particles have a slightly narrower distribution. The average diameter $\bar{d}$ and standard deviation Δd are indicated on each subfigure. The variation coefficient $\bar{d}/\Delta d$ is at most 6%. Since our measurements are very close to the manufacturer's data, in the main text we refer to the particle using their rounded diameter (*e.g.* 20 μm instead of 21.6 μm). The real value is used for calculations.
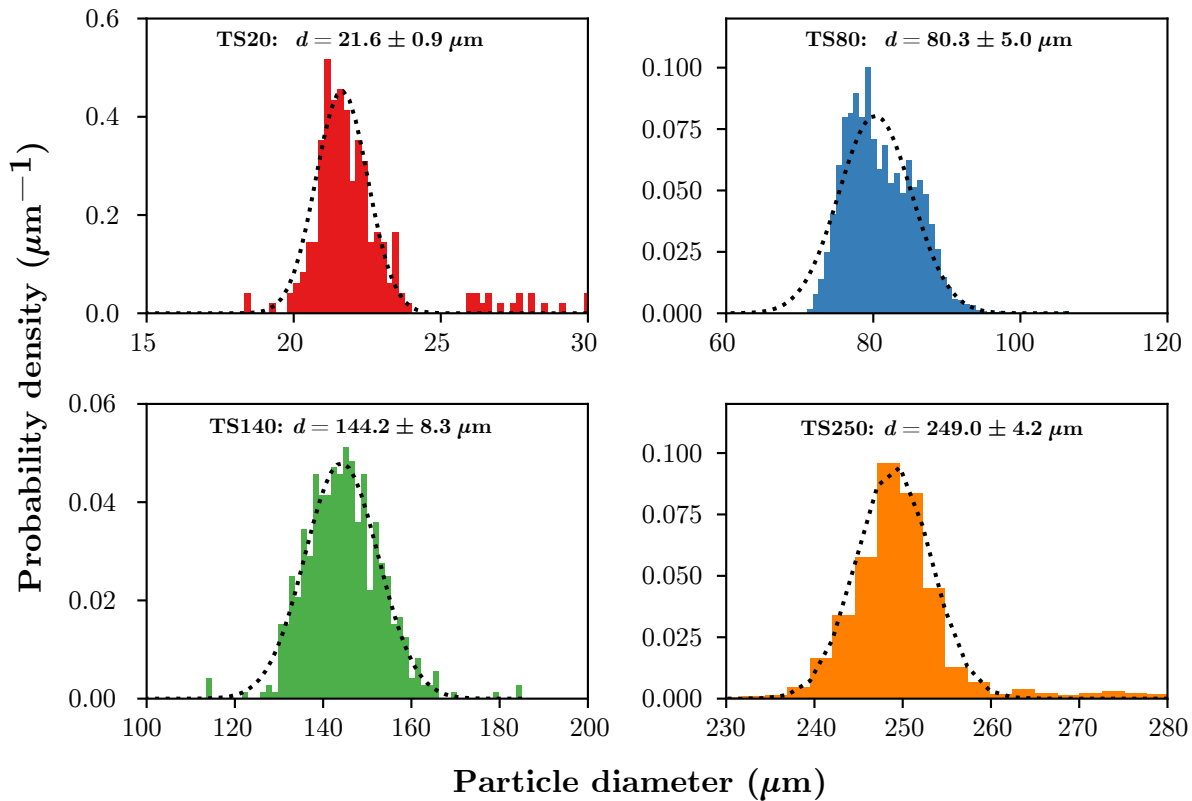

FIG. 7. Size distribution of the polystyrene beads. The dotted line is the best fit by a Gaussian law.

[1] V. Thiévenaz and A. Sauret, Physical Review Fluids **6**, L062301 (2021).
[2] S. Rajesh, V. Thiévenaz, and A. Sauret, Soft Matter **18**, 3147 (2022).
[3] N. Ouchiyama and T. Tanaka, Industrial & Engineering Chemistry Fundamentals **20**, 66 (1981).
[4] N. Ouchiyama and T. Tanaka, Industrial & Engineering Chemistry Fundamentals **23**, 490 (1984).
[5] P. Gondret and L. Petit, Journal of Rheology **41**, 1261 (1997).
[6] V. Thiévenaz, S. Rajesh, and A. Sauret, Soft Matter **17**, 6202 (2021).
[7] S. Pednekar, J. Chun, and J. F. Morris, Journal of Rheology **62**, 513 (2018).
[8] C. Chang and R. L. Powell, Journal of Rheology **38**, 85 (1994).